Title

Extraction of Blebs in Human Embryonic Stem Cell Videos

Journal

IEEE/ACM Transactions on Computational Biology and Bioinformatics, 13(4)

ISSN

1545-5963

Authors

Guan, Benjamin X

Bhanu, Bir

Talbot, Prue

et al.

Publication Date

2016

DOI

10.1109/tcbb.2015.2480091

Peer reviewed

Extraction of Blebs in Human Embryonic Stem Cell Videos

Benjamin X. Guan*, *Student Member, IEEE*, Bir Bhanu*, *Fellow, IEEE*
Prue Talbot** and Nikki Weng**

Abstract— Blebbing is an important biological indicator in determining the health of human embryonic stem cells (hESC). Especially, areas of a bleb sequence in a video are often used to distinguish two cell blebbing behaviors in hESC; dynamic and apoptotic blebbings. This paper analyzes various segmentation methods for bleb extraction in hESC videos and introduces a bio-inspired score function to improve the performance in bleb extraction. Full bleb formation consists of bleb expansion and retraction. Blebs change their size and image properties dynamically in both processes and between frames. Therefore, adaptive parameters are needed for each segmentation method. A score function derived from the change of bleb area and orientation between consecutive frames is proposed which provides adaptive parameters for bleb extraction in videos. In comparison to manual analysis, the proposed method provides an automated fast and accurate approach for bleb sequence extraction.

Index Terms— Bleb extraction, bioinformatics, bio-inspired, human embryonic stem cell (hESC).

1 Introduction

Blebs are membrane protrusions that appear and disappear from the surface of cells. The extraction of blebs and their changing area over time in live videos is important for understanding the mechanisms and function of human embryonic stem cell (hESC) blebbing behavior. The nature of blebbing behavior can be used to evaluate cell health-dynamic blebs indicate healthy cells and apoptotic blebs indicate dying cells. The ability to analyze rates of bleb formation and retraction are important in the field of toxicology and could form the basis of an assay that depends on a functional cytoskeleton [1] [2] [3]. The biologists attempt to clarify the difference between dynamic and apoptotic blebbings in hESC by comparing the time of their occurrences. Blebbing is considered to be related to signaling pathways. It is significant for biologists to have enough evidence to determine whether Calcium, ATP and P2X7 inhibitors can change the blebbing behavior through the Rho-Rock Pathway or not. Inhibitors can alter blebbing behavior by either blocking the pathway leading to myosin activation or inhibit myosin directly. The dynamic segmentation of blebs enables a rapid analysis to make quantified measurements on very large datasets collected with hESC under different experimental conditions. This will lead to the understanding of foundational mechanisms and function of blebbing which can ultimately control/regulate dynamic blebbing in hESC.

Two types of bleb characterization are needed to be understood: Image characterization and physical characterization of blebs. Image characterization of blebs requires the development of computational methods that can provide high detection accuracy with minimum user interaction with blebs in video. Physical characterization of blebs provides enormous understanding of the dynamic cell behavior. For example, it enables the development of a method to prevent blebbing behaviors that lead to cell death. Bleb detection in video is a way to accelerate our understanding of blebs for the development of its physical characterization.

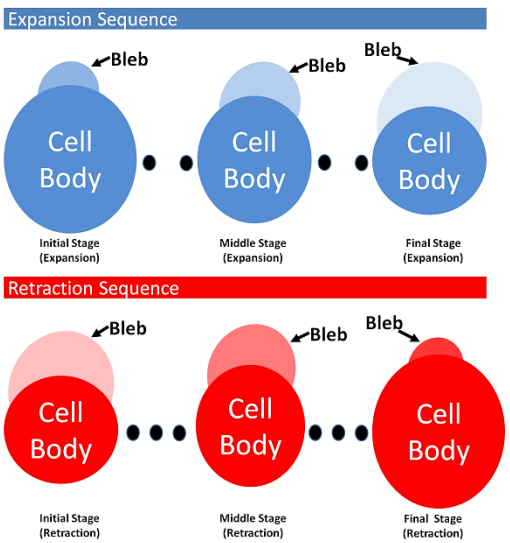

Fig. 1. Expansion and retraction processes occuring over time.

This paper uses the H9 line of hESC (WiCell, Madison, WI.) which are normally about 10 microns in diameter. The average bleb-to-cell body ratio is about 16:57. In 2D images, a single cell can have an average of 6 or a maximum of 11 blebs with a 20x objective. This paper is in-

* *B.X. Guan and B. Bhanu are with the Center for Research in Intelligent Systems and the Department of Electrical and Computer Engineering, University of California-Riverside, Riverside, CA 92521 USA (e-mail: xguan001@ucr.edu; bhanu@cris.ucr.edu).*
** *P. Talbot and N. Weng are with the Stem Cell Center, University of California Riverside, Riverside, CA 92521 USA (e-mail: talbot@ucr.edu; jweng002@ucr.edu).*

tended to explain the bleb formation phenomena and to introduce a method to segment sequences of bleb regions in video for further analysis. Bleb formation consists of two processes: 1) expansion; 2) retraction [4] [5]. In the first stage, the bleb expands sporadically. During the retraction stage, the bleb either retracts back and disappears or partially retracts. Complete bleb retraction normally occurs during dynamic blebbing, which is a characteristic of healthy cells. However, if bleb retraction does not occur or occurs slowly, the cell is likely undergoing apoptosis or cell death. Fig. 1 shows the sequences of both bleb expansion and retraction. During expansion, bleb size increases while cell body size decreases. In contrast, during bleb retraction, bleb size decreases while cell body size increases. At the final stage of expansion, the bleb is called an *intermediate bleb*. The intermediate bleb indicates that transition from expansion to retraction is occurring. The intermediate bleb has the maximum bleb size in full bleb formation process.

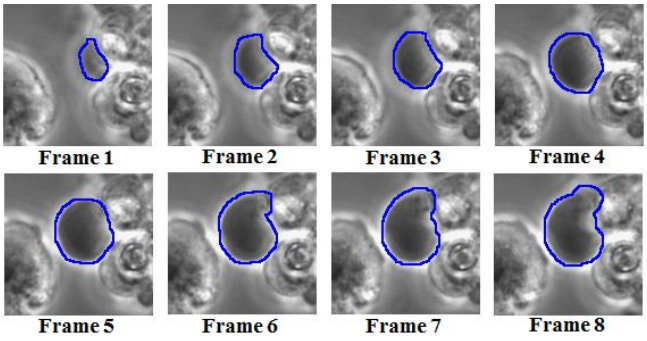

Fig. 2. Example of bleb expansion sequence.

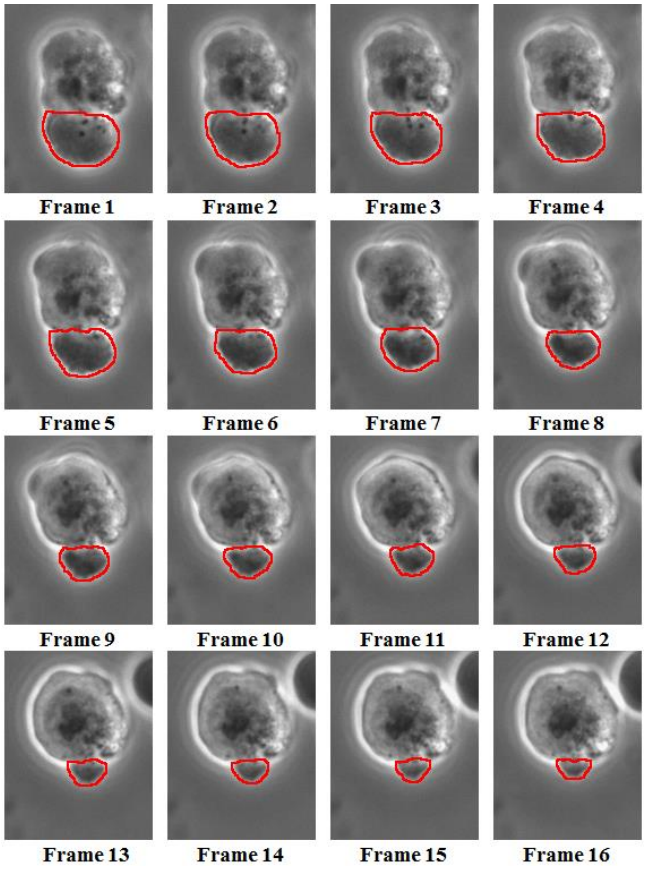

Fig. 3. Example of bleb retraction sequence.

Fig. 2 and 3 show phase contrast images of blebbing sequences for both expansion and retraction. The expansion and retraction processes are visually similar but biologically distinct [6] [7]. Based on our observation on the videos, the change in area and orientation between blebs from the consecutive frames are important for the segmentation of blebs. With the modeled distributions of the change in area and orientation, adaptive parameters for segmentation methods are possible. Additionally, segmentation methods with adaptive parameters improve the performance in the detection of blebs.

Section 2 presents related work and the contributions of this paper. Section 3 describes the technical approach in detail. Section 4 provides experimental results and discussions on video data. Finally, Section 5 provides the conclusions of the paper.

2 Related Work And Contributions

2.1 Blebbing of Human Embryonic Stem Cell

Both hESC dynamic and apoptotic blebbings consist of two processes: expansion and retraction. From our previous studies, we observed that hESC tends to have more blebs as well as having a higher rate of blebbings. Apoptotic blebblings in non-healthy cells are commonly studied. However, blebs exist in both healthy and non-healthy cells. Therefore, it is essential to analyze dynamic blebbings in healthy cells. Understanding the differences between both dynamic and apoptotic blebbings' mechanism and function can lead to a breakthrough in development of regenerative medicine.

2.2 Computational Models for Blebbing

Charras et al. [4] [5] reasoned that blebbing depends on parameters such as pressure, membrane-cortex, adhesion energy and membrane tension of a cell. The plasma membrane of a hESC is attached under tension to a cortex of filaments. If the connection with the filaments is weakened, a bleb is produced by an event of pouring cytoplasmic fluid into the weakened region. When the growth of the bleb stops, the bleb either retracts or stays the same. If an actin cortex reforms under the bleb membrane, retraction is likely to occur and is driven by myosin-II.

StryChalski et al. [6] assumed that blebbing occurs due to detachment of the cytoskeleton from the plasma membrane, which produces a pressure-driven flow of cytosol toward the area of detachment and into the area of expansion. They proposed a computational model of blebbing based on the mechanics of intracellular fluid, the actin cortex, and the cell membrane. The model considers the bleb formation time as a function of parameters derived from cytoplasmic properties [6]. A similar model has been proposed in [7].

2.3 Detection and Segmentation Methods for Cells

Due to the abundance, heterogeneity, dimensionality and complexity of the image data, manual image processing

and analysis is not feasible. In the analysis of biological images, the performance of a segmentation method heavily depends on the tuning of segmentation parameters [8]. It is a tedious process yet the tuned parameters do not guarantee the same performance on similar images. Object detection and segmentation are essential in the analysis of hESC and they are closely related.

Guan et al. [9] [10] present bio-inspired detection/segmentation methods for hESC in phase contrast images. Their segmentation method was developed based on the image property differences between cell region and background [10]. Yin et al. [11] also developed a cell segmentation method by using a bag of local Bayesian classifier. Their segmentation method classifies each pixel in a region with a Bayesian classifier. However, both methods only work for extraction of cell and cell colony from a phase contrast video. In this paper, we are concerned with the detection of blebs of a single cell. Note that blebs are part of the cell with similar image properties. Since there is no previous work on detection of blebs, we will exploit the following four commonly used methods for image segmentation: *region growing*, *normalized cut*, *meanshift* and *watershed*.

Region growing (RG) by Adams et al. [12] [13] grows a region initially from a seed point and groups its neighboring pixels to its region based on their similarity coefficient threshold. *Normalized cut (NC)* method by Shi et al. [14] is a graph based approach, and performs segmentation by maximizing association within groups while minimizing disassociation between groups. *Meanshift (MS)* method by Comaniciu et al. [15] is a well-known density based approach that partitions the image by assigning pixels into clusters with the same mode [16] [17]. *Watershed (WS)* method performs a flooding process on a gradient image where it starts at a local minima and builds watersheds to separate adjacent catchment basins [18] [19].

2.4 Challenges for Bleb Analysis

Since a bleb is part of the cell, it brings the following challenges: i) bleb intensity and texture vary for different cells; ii) blebs are connected to the cell body; iii) blebs have similar intensity/texture as the cell body or background; iv) neighboring blebs share similar intensity and texture. Fig. 4 shows a set of expanding and retracting blebs. Although these blebs look similar, they are different from each other in intensity and texture. Therefore, the conventional segmentation methods with constant parameters will not work well on all the bleb images in a video. Most importantly, blebbing is a dynamic process, and the bleb properties change over time. As a result, subsequent blebs in the same video sequence might have different image properties. Consequently, the performance of *RG*, *NC*, *MS* and *WS* methods will suffer from any constant input parameters.

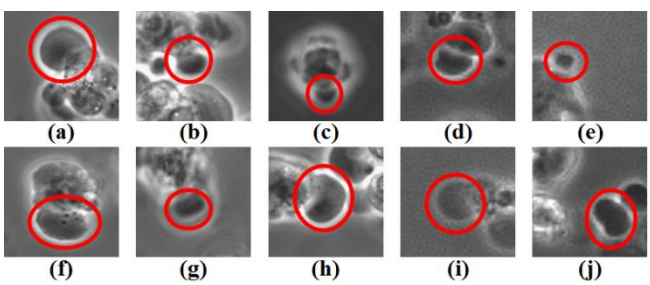

Fig. 4. A sample of blebs. (Note: the variety of blebs that are circled in these images)

TABLE 1
DEFINITION OF THE SYMBOLS USED IN THIS PAPER

Symbol	Definition
t	Index for the distribution functions.
$E(t; A_E)$	Exponential distribution function.
A_E	Inverse scaling parameter of the exponential.
$G(t; A_G, B_G)$	Gaussian distribution function.
A_G	Mean for the Gaussian distribution.
B_G	Standard deviation for the Gaussian distribution.
$LN(t; A_{LN}, B_{LN})$	Lognormal distribution function.
A_{LN}	Location parameter of the lognormal.
B_{LN}	Scale parameter of the lognormal.
$\mathcal{P}(t; A_{\mathcal{P}})$	Poisson distribution function.
$A_{\mathcal{P}}$	Mean parameter of the Poisson.
$RL(t; A_{RL})$	Rayleigh distribution function.
A_{RL}	Mode parameter of the Rayleigh distribution.
$GAM(t; A_{GAM}, B_{GAM})$	Gamma distribution function.
A_{GAM}	Shape parameter of the Gamma distribution.
B_{GAM}	Scale parameter of the Gamma distribution.
$S_{\alpha,\phi}(\Delta A, \Delta\theta)$	Bio-inspired optimization metric.
$\Delta A, \Delta\theta$	Values for change in bleb area and orientation.
α	Parameters vector of modeled ΔA distribution.
ϕ	Parameters vector of modeled $\Delta\theta$ distribution.

2.5 Contributions of this Paper

We propose a bio-inspired optimization method for the segmentation of dynamic blebs. The proposed approach adapts parameters for images in the bleb formation process: expansion and retraction. The parameters for the bio-inspired metric are derived directly from the distributions of change in area and orientation between consecutive blebs. Since the health status of a cell can be determined from the bleb formation process, it is important to improve the accuracy in bleb detection. Therefore, the proposed optimization method is essential in quantitative analysis of cell health.

3 TECHNICAL APPROACH

In this section, we first introduce the derivation of the statistical models for bio-inspired optimization metric. We also elaborate on the optimization metric. We then explain the segmentation methods for the detection of blebs in video. In addition, a summary of the proposed algorithm and a flowchart for segmentation in video are also provided. For the convenience of the reader, a summary of the symbols used in this paper is given in Table 1. Fig. 5 shows the overview of the proposed system.

The proposed system uses exhaustive search to obtain an optimal solution. Segmentation result with specific parameters is given a score in the bio-inspired optimization step. This score is calculated based on the modeled distributions. The modeled distributions are the general-

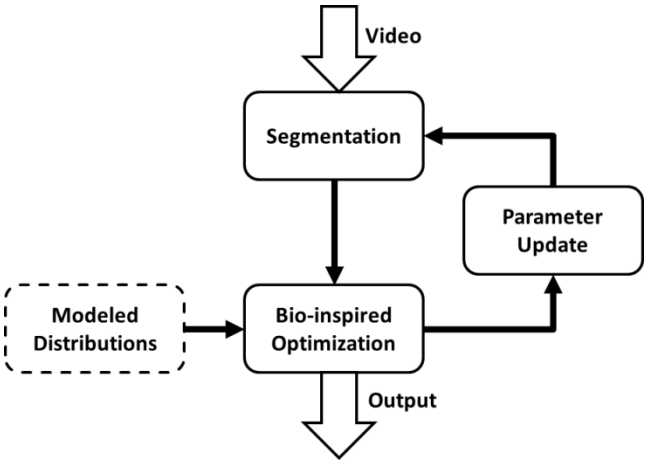

Fig. 5. Overview of the proposed system.

ized distributions obtained from distribution fitting the change in bleb areas and orientations.

3.1 Modeled Distributions

3.1.1 Motivation

Since image properties of a bleb changes with time, constant parameters of segmentation methods will perform poorly. Therefore, dynamic parameters with consideration of bleb changes over time are needed for the segmentation methods. Based on our observation of the hESC blebbing videos, we concluded that ΔA and $\Delta\theta$ between consecutive frames provide relative behavior of a bleb over time. Fig. 1 shows an example of how bleb changes over time. Therefore, we obtain the generalized models for ΔA and $\Delta\theta$ distributions through model fitting.

3.1.2 Learning the Distributions of ΔA and $\Delta\theta$

We used a model fitting technique on the actual distributions of ΔA and $\Delta\theta$. Equations (1)-(6) are used in our model fitting technique [20] [21]. Definitions of parameters for the following equations are provided in Table 1.

Exponential distribution function:

$$E(t; A_E) = A_E e^{-A_E t} \tag{1}$$

Gaussian distribution function:

$$G(t; A_G, B_G) = \frac{1}{B_G\sqrt{2\pi}} e^{-\frac{(t-A_G)^2}{2B_G^2}} \tag{2}$$

Lognormal distribution function:

$$LN(t; A_{LN}, B_{LN}) = \frac{1}{tB_{LN}\sqrt{2\pi}} e^{-\frac{(\ln(t)-A_{LN})^2}{2B_{LN}^2}} \tag{3}$$

Poisson distribution function:

$$\mathcal{P}(t; A_{\mathcal{P}}) = \frac{A_{\mathcal{P}}^t}{t!} e^{-A_{\mathcal{P}}} \tag{4}$$

Rayleigh distribution function:

$$RL(t; A_{RL}) = \frac{t}{{A_{RL}}^2} e^{\frac{-t^2}{2A_{RL}^2}} \tag{5}$$

Gamma distribution function:

$$GAM(t; A_{GAM}, B_{GAM}) = \frac{1}{\Gamma(A_{GAM}) B_{GAM}^{A_{GAM}}} t^{A_{GAM}-1} e^{-\frac{t}{B_{GAM}}} \tag{6}$$

$\Gamma(*)$ is a gamma function operator. The optimal parameters and mean squared error (MSE) for each distribution is shown in Table 2. Since we are seeking model that yields low MSE for each distribution, we conclude that both ΔA and $\Delta\theta$ can be characterized as Gamma distributions. Fig. 6 shows the best models that fit the actual ΔA and $\Delta\theta$ distributions.

TABLE 2
MODELED DISTRIBUTIONS: PARAMETERS AND MSE

Parameters and MSE for ΔA Distribution

Parameters	Exp.	Gauss.	Log.	Poisson	Rayleigh	Gamma
A	61.810	61.810	2.617	61.810	103.134	**0.431**
B	'NA'	132.356	2.983	'NA'	'NA'	**143.288**
MSE	1.07E-03	1.43E-03	9.48E-04	2.10E-03	1.77E-03	**9.29E-04**

Parameters and MSE for Δθ Distribution

Parameters	Exp.	Gauss.	Log.	Poisson	Rayleigh	Gamma
A	19.474	19.474	0.970	19.474	31.116	**0.338**
B	'NA'	39.535	4.369	'NA'	'NA'	**57.574**
MSE	4.29E-03	6.25E-03	4.11E-03	8.80E-03	8.31E-03	**3.60E-03**

Note: A and B → parameters for each model distribution;
MSE → mean squared error; Bold → best result ; Exp. → Exponential;
Gauss. → Gaussian; Log. → Lognormal; NA → not applicable.

3.2 Bio-inspired Optimization for Segmentation

For this paper, the segmentation methods with the bio-inspired optimization are called *bio-optimized* methods. The bio-inspired optimization metric provides an adaptive solution to the segmentation problem with following two steps. First, the metric yields scores for a set of parameters in a particular segmentation method and retains the corresponding scores of the parameters in the set. Second, optimal solution is selected from the parameters with the highest score.

3.2.1 Bio-inspired Optimization Metric

The optimization metric $S_{\alpha,\phi}(\Delta A, \Delta\theta)$ considers D_1 and D_2, the modeled ΔA and $\Delta\theta$ distributions, as two independent distributions. $D_1(\Delta A; \alpha)$ is a score of ΔA in a distribution that is parameterized by α. $D_2(\Delta\theta; \phi)$ is a score of $\Delta\theta$ in a distribution that is parameterized by ϕ. The general form of the optimization metric is shown below.

$$S_{\alpha,\phi}(\Delta A, \Delta\theta) = D_1(\Delta A; \alpha) * D_2(\Delta\theta; \phi) \tag{7}$$

The final form of the optimization metric is shown in the following equation:

$$S_{max} = \max_{\Delta A, \Delta\theta} S_{\alpha,\phi}(\Delta A, \Delta\theta) \tag{8}$$

The optimized $S_{\max}$ is found when the metric score is maximized with a given ΔA and $\Delta\theta$ values.

3.2.2 Parameter Update

The initial centroid and area of the bleb are given by the end user. Bleb centroid tells the algorithm about the region of interest. Bleb area is needed to calculate ΔA and $\Delta\theta$ for the segmentation parameters. The subsequent bleb centroid and bleb area in a video sequence are generated automatically. The bleb centroid of the next frame is the centroid of the current detected bleb region [22]. Moreover, the assumption of smooth/gradual transition between consecutive frames is made for bleb formation processes. The detected bleb at each frame is a region where the optimal parameters of a segmentation method that maxim-

ized the bio-inspired optimization metric which is described in equation (8). Equation (8) uses the modeled distributions as shown in Fig. 6 to calculate the scores for the segmentation parameters. When the maximum score is found, the estimated bleb centroid and current bleb area for the next frame are updated. The output of the method for a video is a sequence of binary masks of the detected blebs.

3.3 Segmentation Methods Compared

In this section, we explain each segmentation method in detail and show how bio-optimization is achieved. We also provide Table 3 which summarizes the search range for each optimization parameter.

TABLE 3
OPTIMIZATION PARAMETERS AND RANGES

Method	Optimizing Parameters	Range of Optimization
Region Growing	Similarity coefficient threshold	0 to 1 with step 0.01
NCUT	Number of clusters	2 to 10 with step 1
Meanshift	Spatial bandwidth	1 to 8 with step 1
	Range bandwidth	1 to 8 with step 1
Watershed	Suppressing value/threshold	1 to 254 with step 1

3.3.1 Region Growing

Region growing is a region based segmentation method. It starts with an initial seed point and iteratively evolves its region by evaluating its region's neighboring contour. It groups the contour pixels based on a similarity threshold. The contour pixels are grouped into the region if the similarity between the pixel and region feature is less than a threshold. As a result, the performance of the region growing method depends on the selection of the threshold. In the bio-optimized region growing approach, the threshold is an adaptive parameter that is needed to be found. The search range for the optimal threshold in the bio-optimized region growing is from 0 to 1 with stepsize 0.01.

3.3.2 Normalized Cut

Normalized cut is a graph based approach. It considers each pixel as a vertex and edge as a connection weight between pixels. The main objective of this approach is to minimize the disassociation between the groups while maximizing the association within the groups. The number of possible groups is determined by the end user. As a result, the number of possible groups in an image is the adaptive parameter in the bio-optimized normalized cut. Since the bleb is the foreground and the rest of the image is the background, we have at least two components in the image. Based on observation, each frame consists of five different regions: 1) background; 2) cell body; 3) halo; 4) bleb; 5) debris or part of neighboring cell. Since the image contains these five basic regions, the number of expected regions is five under ideal condition. With the consideration of the worst case scenario, we double the number of possible components in an image. Therefore, the search range is set to be 2 to 10 components.

3.3.3 Meanshift

Meanshift method is a density based approach. It has two parameters: spatial and range bandwidths. It also requires the minimum size of a region. In this paper, the minimum size of a region is set to be 60 pixels which is the smallest recognizable bleb. The spatial range determines the size of the search window that computes the meanshift. The range bandwidth determines the window size that is used to compute the feature. In this paper, the optimization search range for the spatial bandwidth is from 1 to 8 and the range bandwidth is from 1 to 8.

3.3.4 Watershed

Watershed is a topological based method. It is often applied on a gradient image. It partitions the image into two different sets: catchment basins and watershed line. The watershed method floods the topographic surface of a gradient image from its regional minima. It builds watershed lines to prevent waters in different catchment basins from merging. In this paper, the gradient image is the Euclidean distance transform of the marker image. The marker im-

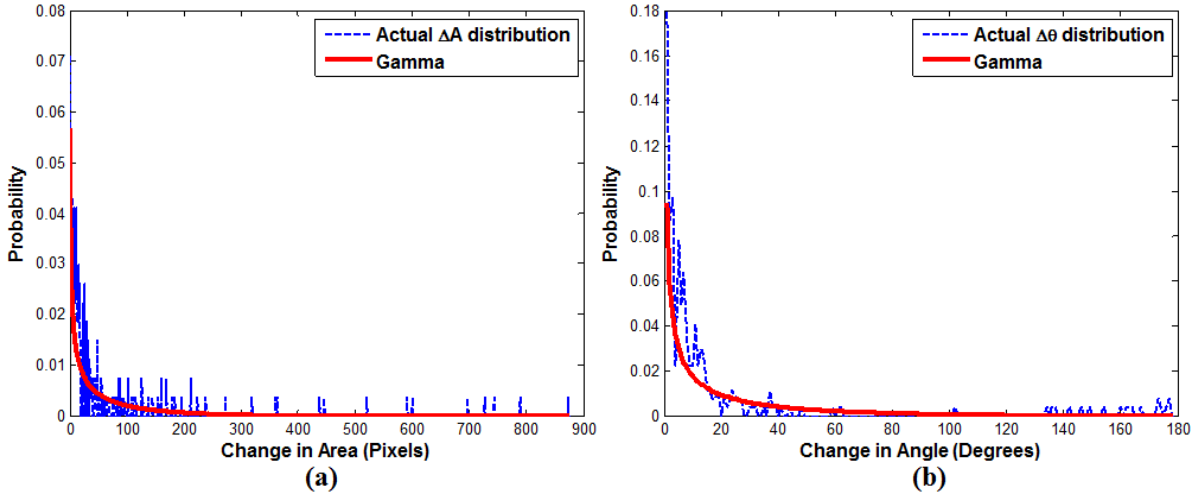

Fig. 6. Modeled fitting for (a) ΔA distribution and (b) $\Delta\theta$ distribution are Gamma. (ΔA and $\Delta\theta$ are derived from both expansion and retraction datasets.)

age (binary image) is obtained with the extended minimum of the original image [19]. The extended minimum approach depends on the suppressing value to binarize the image. Therefore, the suppressing value is the adaptive parameter for the bio-optimized watershed. Since the image is an 8 bit image, the search range for the optimal suppressing value is from 1 to 254.

3.4 Summary of the Proposed Algorithm

Algorithm 1 Bleb extraction in video

Input: V is a video with a total F number of frames. B_{cent} and B_{area} are given bleb centroid and area initially.
Output: R is a sequence of binary masks of blebs.

1: **procedure** BlebExtraction(V, B_{cent} , B_{area})
2: Set frame index f to 1.
3: Perform segmentation with different segmentation parameters on f_{th} video frame, $V(f)$.
4: Obtain optimal parameters/segmentation result by equation (8)
5: Save optimal segmentation result to $R(f)$
6: Update estimated B_{cent} and B_{area} with $R(f)$
7: Increment frame index f by 1.
8: Repeat steps 3 to 7 until index $f > F$
9: Output segmentation result R.
10: **end procedure**

To further explain the segmentation block as shown in Fig. 5, a flow chart of segmentation is provided in Fig. 7. It shows a general process of segmentation with a set of parameters for a single bleb.

4 Experimental Results

4.1 Data

All time lapse videos were obtained with a BioStation IM [23] [24]. The frames in the video are phase contrast images. The videos were acquired using 20x objective with 600 x 800 resolution. Each video frame is acquired at 2 seconds time interval. For this experiment, we have 26 expansion, 30 retraction, and 9 full bleb formation videos which are cropped randomly from the BioStation's raw videos. A total of 692 frames are in the 65 videos. The ΔA and $\Delta\theta$ distributions are derived from the first 13 expansion and 15 retraction videos. The remaining 13 expansion, 15 retraction and 9 full bleb formation videos are used as the testing dataset. The ground-truth for all videos was generated manually by expert biologists.

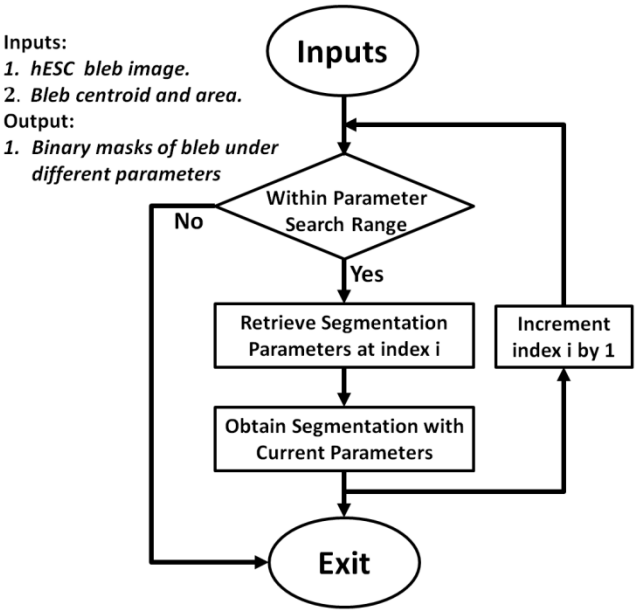

Fig. 7. Flowchart for segmentation

4.2 Parameters

4.2.1 Segmentation Parameters of Standard Algorithms

The conventional segmentation parameters are identified individually by a receiver operating characteristic (ROC) curve [25]. Fig. 8 shows the ROC curves for four different segmentation methods. The training frames are obtained from the first frame of each 28 experimental videos. The optimal point is the maximum true positive rate within the range of 0 to 0.4 false positive rates. Based on the ROC, we determined that the region growing's optimal similarity threshold is set to be 0.15. For the normalized cut method, the optimal number of components is 2. For meanshift, optimal range and spatial bandwidths are 1 and 3. Its minimum region criterion is set to 60 pixels which is the smallest recognizable bleb size. For watershed, the optimal suppressing value is 115.

4.2.2 Parameters for the Proposed Method

For the proposed method, the first bleb area and center were needed initially for each video sequence and were provided by the end user. The modeled distribution parameters are also required for the bio-inspired optimization metric. Since ΔA and $\Delta\theta$ distributions are best fitted by Gamma distribution with different parameters, we uses their optimal parameters in the optimization metric.

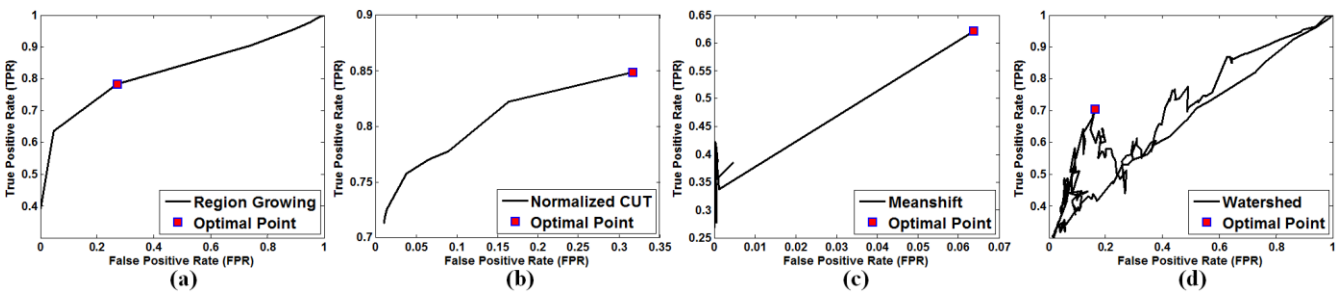

Fig.8. ROC plot for (a) Region growing, (b) normalized CUT, (c) meanshift, (d) watershed.

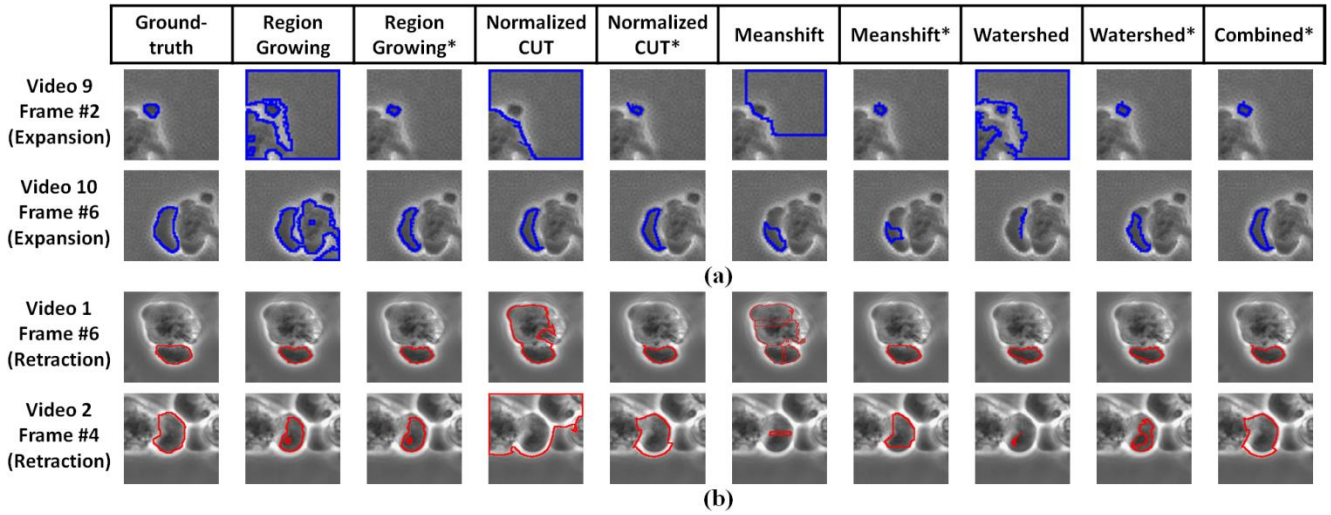

Fig.9. Visual comparisons of four different blebs with results from (a) expansion process and (b) retraction process. (Note that frames from two sets of videos are used in the figure: expansion and retraction videos. Expansion results are outlined in blue and retraction results are outlined in red.)

ΔA distribution is modeled as Gamma distribution with parameters A_{GAM} and B_{GAM} equal to 0.431 and 143.288. $\Delta\theta$ distribution is also modeled as a Gamma distribution with parameters A_{GAM} and B_{GAM} equal to 0.338 and 57.574. The aforementioned model parameter values are used in equations (7) and (8).

There are two different types of parameters that need to be considered for our approach: (a) the parameters of the optimization metric and (b) the range of parameters of the selected segmentation method. For the optimization metric parameters, the parameter sensitivity depends on the size and the quality (independent samples, image quality, etc.) of the representative dataset. Typically, a larger training dataset can better generalize the parameters in the optimization metric. For each segmentation method, the range of parameter values depends on the method and the characteristics of video frames. For this paper, a detailed discussion is provided in Subsections 3.3 and 4.2 to determine the parameter range for each segmentation method. This range provided good segmentation results for the videos used in this paper.

4.3 Performance Measures

For comparison, we use methods suggested by Shattuck et al. [25][26]. Our comparison metrics are Jaccard similarity (JAC), Dice coefficient (DIC), sensitivity (SEN), specificity (SPC) and balanced accuracy (BAC). The JAC is a measure of similarity between experimental results and the ground-truth. The DIC is the measure of the agreement between experimental results and ground-truth. The SEN is a measurement of the proportion of actual positives which are correctly identified. The SPC measures the proportion of the actual negatives which are correctly identified. Moreover, the true positive rate (TPR) is equivalent to SEN, and the false positive rate (FPR) is same as SPC subtracted from 1. The BAC is an average of SEN and SPC. The equation for each metric is shown below:

$$JAC = \frac{TP}{(TP+FP+FN)} \quad (9)$$

$$DIC = \frac{2TP}{(2TP+FP+FN)} \quad (10)$$

$$SEN = \frac{TP}{(TP+FN)} \quad (11)$$

$$SPC = \frac{TN}{(FP+TN)} \quad (12)$$

$$BAC = \frac{SEN+SPC}{2} \quad (13)$$

The variables are defined as follows: 1) true positive (TP), 2) true negative (TN), 3) false positive (FP) and 4) false negative (FN). TP indicates the overlapped region of the detected bleb's binary mask and the bleb ground-truth's binary mask. TN is the overlapped region of the detected background's binary mask and the background ground-truth's binary mask. FP is the detected background's binary mask that is falsely identified as part of the bleb region. FN is the detected bleb's binary mask that is falsely identified as part of the background.

4.4 Segmentation Results

4.4.1 Qualitative Results

The bio-inspired optimization on all segmentation methods, combined bio-optimized method, has better performance on average than other methods as shown in Fig. 9. All bio-optimized methods have segmentation results closer to the ground-truth. Since the segmentation with the bio-optimized methods is constrained by the bio-optimization metric, over-segmentation was less significant than the conventional methods.

4.4.2 Quantitative Results

The segmentation methods with the bio-inspired optimization outperformed all conventional segmentation methods in this paper. The conventional meanshift with fixed parameters outperforms the other conventional segmentation methods. Based on average mean JAC and average mean DIC of the three datasets, the bio-optimized meanshift outperformed the conventional meanshift by more than 12%. In addition, all other bio-optimized methods outperformed their conventional counterparts by at least 5% in both mean JAC and mean DIC. The mean JAC and mean DIC performances for each dataset are shown in Table 4.

The top four performers based on the average mean JAC and average mean DIC of the three datasets are ranked as combined bio-optimized method, bio-optimized region growing, bio-optimized meanshift and bio-optimized watershed. Table 5 shows corresponding average mean JAC and average mean DIC for the aforementioned top performers. The combined bio-optimized method is the best performer in all datasets. The combined bio-optimized method also has 79.19% in average mean BAC which is the best overall performance in all

TABLE 4
RESULTS ON EXPERIMENTAL DATA (NOTE ALL VALUES ARE IN PERCENTAGE)

Results on Expansion Videos

Metric	JAC				DIC				SEN				SPC			
Method	**Min**	**Max**	**Std**	**Mean**	**Min**	**Max**	**Std**	**Mean**	**Min**	**Max**	**Std**	**Mean**	**Min**	**Max**	**Std**	**Mean**
Region Growing	2.02	77.96	26.42	21.92	3.95	87.61	29.36	30.16	68.75	99.86	9.27	84.09	3.00	99.97	40.49	49.04
Region Growing*	**43.22**	**80.69**	**12.97**	**60.11**	**60.35**	**89.31**	**10.12**	**74.33**	**43.22**	**81.18**	**12.59**	**63.73**	**95.56**	**100.00**	**1.38**	**99.44**
NCUT	1.97	62.11	20.49	21.75	3.86	76.62	25.05	31.87	58.87	100.00	15.24	78.43	2.86	100.00	35.73	61.18
NCUT*	9.58	62.07	20.16	42.90	17.48	76.59	21.97	57.19	55.17	83.62	9.14	67.71	85.61	100.00	5.12	95.48
Meanshift	2.57	69.74	20.84	39.78	5.01	82.18	23.74	53.68	46.25	73.55	8.89	60.95	35.84	100.00	17.58	90.94
Meanshift*	**29.83**	**73.70**	**13.67**	**55.24**	**45.95**	**84.86**	**12.02**	**70.19**	**29.89**	**77.36**	**14.63**	**58.62**	**96.93**	**100.00**	**0.82**	**99.59**
Watershed	3.89	61.10	18.21	21.99	7.50	75.85	22.37	32.99	43.11	100.00	18.61	76.91	23.51	98.77	22.81	73.91
Watershed*	**27.55**	**73.99**	**15.17**	**45.99**	**43.20**	**85.05**	**14.00**	**61.67**	**27.55**	**78.63**	**17.69**	**51.14**	**96.21**	**100.00**	**1.16**	**99.14**
Combined*	**45.06**	**78.87**	**9.05**	**60.68**	**62.13**	**88.18**	**7.05**	**75.17**	**48.12**	**81.18**	**9.76**	**65.30**	**96.30**	**100.00**	**0.99**	**99.54**

Results on Retraction Videos

Metric	JAC				DIC				SEN				SPC			
Method	**Min**	**Max**	**Std**	**Mean**	**Min**	**Max**	**Std**	**Mean**	**Min**	**Max**	**Std**	**Mean**	**Min**	**Max**	**Std**	**Mean**
Region Growing	4.68	32.64	8.39	12.78	8.94	49.22	12.36	21.80	63.59	98.30	8.97	81.43	4.71	86.57	30.18	53.22
Region Growing*	**15.21**	**74.55**	**14.86**	**57.26**	**26.41**	**85.42**	**14.65**	**71.54**	**37.82**	**74.57**	**9.63**	**62.31**	**76.12**	**100.00**	**6.12**	**98.22**
NCUT	2.69	16.66	4.15	10.95	5.24	28.57	6.85	19.50	66.24	100.00	11.66	84.78	5.78	82.21	22.09	51.10
NCUT*	14.30	62.62	13.31	43.20	25.03	77.01	13.98	59.13	47.47	86.69	11.76	62.90	78.70	99.95	6.67	95.51
Meanshift	4.82	70.87	20.30	42.23	9.21	82.95	21.73	56.52	41.91	76.04	10.12	59.96	77.12	100.00	6.74	95.34
Meanshift*	**41.63**	**73.77**	**9.22**	**58.30**	**58.78**	**84.90**	**7.53**	**73.25**	**46.53**	**76.84**	**7.99**	**60.97**	**99.02**	**100.00**	**0.28**	**99.77**
Watershed	5.73	49.89	14.23	22.22	10.83	66.57	18.07	34.40	32.34	94.16	19.34	62.27	53.77	98.63	15.08	82.52
Watershed*	**26.62**	**68.73**	**13.41**	**47.59**	**42.04**	**81.47**	**12.84**	**63.40**	**28.08**	**78.80**	**15.09**	**52.63**	**97.83**	**100.00**	**0.75**	**99.21**
Combined*	**41.63**	**73.77**	**9.42**	**59.92**	**58.78**	**84.90**	**7.60**	**74.52**	**49.48**	**82.05**	**10.41**	**65.73**	**96.35**	**100.00**	**1.00**	**99.32**

Results on Full Bleb Formation Videos

Metric	JAC				DIC				SEN				SPC			
Method	**Min**	**Max**	**Std**	**Mean**	**Min**	**Max**	**Std**	**Mean**	**Min**	**Max**	**Std**	**Mean**	**Min**	**Max**	**Std**	**Mean**
Region Growing	1.25	21.45	6.60	5.07	2.47	35.33	10.78	9.05	62.65	91.32	8.55	78.76	2.83	96.43	33.70	55.73
Region Growing*	**9.71**	**55.08**	**13.71**	**40.79**	**17.70**	**71.03**	**16.15**	**56.56**	**11.45**	**55.28**	**13.11**	**41.94**	**99.60**	**100.00**	**0.13**	**99.93**
NCUT	1.44	4.08	0.84	2.49	2.85	7.85	1.60	4.84	87.05	100.00	4.55	97.22	1.43	77.52	19.56	45.31
NCUT*	1.47	36.22	15.49	16.95	2.89	53.18	22.62	26.33	50.05	99.67	21.48	73.29	1.43	99.53	35.23	71.28
Meanshift	3.57	48.78	17.02	37.46	6.90	65.58	21.82	52.10	16.04	56.30	12.18	47.85	83.05	99.93	5.57	97.90
Meanshift*	**11.15**	**55.79**	**13.02**	**43.33**	**20.06**	**71.62**	**15.36**	**59.23**	**14.02**	**56.62**	**12.54**	**44.46**	**99.42**	**100.00**	**0.19**	**99.92**
Watershed	2.81	64.93	20.20	17.24	5.47	78.74	24.10	25.75	19.48	88.07	19.07	64.57	76.63	99.77	8.44	90.86
Watershed*	**13.52**	**58.35**	**19.19**	**33.97**	**23.82**	**73.70**	**21.17**	**48.03**	**17.72**	**69.68**	**20.19**	**37.56**	**98.08**	**100.00**	**0.62**	**99.71**
Combined*	**11.15**	**55.79**	**13.14**	**44.07**	**20.06**	**71.62**	**15.51**	**59.92**	**14.02**	**56.62**	**12.62**	**45.24**	**99.42**	**100.00**	**0.19**	**99.92**

* denotes a bio-optimized method and bold denote the top four performers. Combined* denotes optimization on all four segmentation methods.

TABLE 5
TOP FOUR PERFORMERS

Measure	Combined*	Region Growing*	Meanshift*	Watershed*
Average Mean JAC	**54.89%**	52.72%	52.29%	42.52%
Average Mean DIC	**69.87%**	67.48%	67.56%	57.70%
Average Mean BAC	**79.17%**	77.59%	77.22%	73.23%

*** denotes a bio-optimized method, and bold denotes best performance.**

three experimental datasets. The combined bio-optimized's average mean BAC shows that at least 79% of bleb and background regions can be accurately retrieved.

To determine the statistical significance of the top four performers (combined*, region growing*, meanshift*, and watershed*) as shown in Table 5, a t-test with 5% significant level for the combined* method against the other three top performers (region growing*, meanshift* and watershed*) is carried out. The t-test was done for DIC measure. We found that the bio-optimized combined method failed to reject the null hypothesis for the bio-optimized region growing and bio-optimized meanshift methods. However, the null hypothesis was rejected for the bio-optimized watershed method. The acceptance of the null hypothesis was due to the fact that the combined* approach favored one individual segmentation method in some experiments. Therefore, it essentially yields the same solution as a particular segmentation method.

Based on Table 4, the bio-optimized methods generally have lower average standard deviation (Std) in both JAC and DIC measures than their counterparts with exceptions of bio-optimized *NC* and bio-optimized *RG*. The conventional *NC* and *RG* have consistent lower performances in both JAC and DIC for all three datasets. Since the cell and the bleb are dynamically changing over time, adaptive parameters that are found with the bio-optimized metric improves the performance and consistency of the segmentation methods significantly. The fixed parameters in the conventional segmentation methods are not sufficient to handle the blebbing sequence where the bleb's image properties change over time.

Due to the bio-optimized metric, the bio-optimized segmentation methods did not suffer from severe over-segmentation. The bio-optimized segmentation methods' solutions are bounded by the bio-optimized metric. Therefore, the bio-optimized segmentation methods have higher performance for the blebbing sequence than the conventional segmentation methods. The constant parameters in the conventional segmentation approaches are the cause for their low performance. The proposed methods with adaptive parameters are able to capture the local region of the bleb more accurately.

TABLE 6
COMPUTATIONAL TIME STATISTICS PER FRAME IN SECONDS

Method	Min	Max	Mean	Std
Region Growing	0.02	1.39	0.32	0.35
Region Growing*	2.42	38.52	12.52	11.99
NCUT	0.29	4.81	1.74	1.48
NCUT*	2.36	47.56	16.49	14.18
Meanshift	0.02	0.17	0.06	0.05
Meanshift*	0.33	3.86	1.22	1.13
Watershed	0.01	0.05	0.02	0.01
Watershed*	1.67	12.79	4.85	3.28
Combined*	6.61	122.54	36.14	35.07

*** denotes a bio-optimized method.**

4.5 Discussion

4.5.1 Effect of Model Parameters on Performance

The parameters that characterized the ΔA and $\Delta\theta$ distributions are essential in the optimization process. Inaccurate model parameter values might lead to either under-segmentation or over-segmentation of the bleb. As a result, the model parameters found through model fitting are important for equation (7) which yields a score for each element in a set of segmentation parameters.

4.5.2 Effect of Bleb and Cell Sizes on Performance

The bleb and cell body size are important for the performance in the optimization process. There are three types of small blebs that have poor performance in the proposed method:

1. Small blebs due to smaller cell (typically a small bleb has roughly 240 pixels or less).
2. Small blebs at the initial stage of the expansion.
3. Small blebs at the final stage of the retraction.

The smaller blebs for any process are not fully developed and often have similar intensity and texture as the cell body. Therefore, over-segmentation is bound to happen if the cell body and its bleb share similar image properties. The proposed method yields a lower value in comparison metric for small blebs. However, larger cells with larger blebs often perform better. A typical large bleb has 1700 or more pixels.

4.5.3 Automation in Segmentation

The bio-optimized segmentation method is a semi-automated approach in which the initial bleb centroid and area is given by the user in the first frame. Automation is done on the subsequent frames in a video for the optimal segmentation result with equation (8). However, it still alleviates the biologist's burden from complete manual extraction of bleb in video for analysis. The proposed yields bleb area distribution and provides the bleb boundary over time. It is a useful data mining approach to help biologist quantify analyses on dynamic and apoptotic blebbing behavior.

4.5.4 Time Complexity

Since the proposed method was an iterative optimization process, it yielded higher time complexity for all bio-optimized segmentation methods. The best performer among the bio-optimized segmentation methods was the combined bio-optimized method. However, it required an average of 36.14 seconds to process a single frame as shown in Table 6. The bio-optimized meanshift was the only bio-optimized method with the lowest time complexity. The tradeoffs between the bio-optimized meanshift and combined bio-optimized method were performance and time complexity. The experiments were done on a

laptop with an Intel(R) Core™ 2 DUO CPU processor that run at 2.53 GHz.

5 Conclusions

The bio-optimized segmentation methods have better performances than their conventional counterparts. Their high performance shows the modeled distributions is significant for segmenting blebs in videos. With the bio-inspired optimization metric, low performance due to over-segmentation is reduced. However, the segmentation method might not generate an ideal/exact solution to optimize the metric tightly due to the fact that a bleb has similar image properties to its cell body. The over-segmentation in the approach is the inability of the segmentation method to discern the bleb from its cell body.

In terms of biological contribution, this paper introduces a new concept that the bleb formation/retraction process can be used as a biological indicator of cell health. Healthy cells retract their blebs back to the cell body, while non-healthy cells do not retract them or retract them slowly. In terms of a computational contribution, this paper suggests a bio-inspired optimization metric to segment bleb regions. We introduced an approach to improve bleb detection accuracy by using adaptive parameters instead of using constant parameters for all bleb frames in a video. The proposed segmentation methods with adaptive parameters found by the bio-inspired optimization metric has consistently higher performance. In the future work, we will consider incorporating shape prior information in our approach for accurate bleb detection [27][28]. Shape prior will introduce shape variability consideration in our approach [27].

This work can be used by biologists to evaluate the state of health of hESC in culture in various experimental conditions. It could be valuable in drug screening and in toxicological studies where short times to an endpoint are desirable, as well as resource and time saving. It may be adaptable in the future to high throughput screening of chemicals and drugs that need to be evaluated for embryotoxicity.

Acknowledgment

This research was supported by National Science Foundation Integrated Graduate Education Research and Training (NSF-IGERT): Video Bioinformatics Grant DGE 0903667 and by Tobacco-Related Disease Research Program (TRDRP): Grant 20XT-0118 and Grant 22RT-0127.

References

[1] S. Lin, et al., "Comparison of the toxicity of smoke from conventional and harm reduction cigarettes using human embryonic stem cells," in *Toxicol Sci.*, vol. 118, pp. 202-212, Aug. 2010.

[2] Z. Zhu and D. Huangfu, "Human pluripotent stem cells: an emerging model in developmental biology," in *Development*, vol. 140, pp. 705-717, 2013.

[3] P. Talbot and S. Lin, "Mouse and human embryonic stem cells: can they improve human health by preventing disease?," in *Current Topics in Medicinal Chemistry*, vol. 11, no. 13, pp. 1638-1652, 2011.

[4] G.T. Charras, et al., "Life and times of a cellular bleb," in *Biophysical Journal*, vol. 94, pp. 1836-1853, March 2008.

[5] J. Tinevez, U. Schulze, G. Salbreux, J. Roensch, J. Joanny and E. Paluch, "Role of cortical tension in bleb growth," in *PNAS*, vol. 106, no. 44, pp.18581-18586, Nov. 2009.

[6] W. Strychalski and R. D. Guy, "A computational model of bleb formation," in *Mathematical Medicine and Biology*, pp. 1-16, Jan. 2012.

[7] F. Y. Lim, Y. L. Koon and K. H. Chiam, "A computational model of amoeboid cell migration," in *Computer Methods in Biomechanics and Biomedical Engineering*, pp. 1-12, Jan. 2013.

[8] E. Meijering, "Cell segmentation: 50 years down the road [life sciences]," in *IEEE Signal Processing Magazine*, vol. 29, no. 5, pp. 140–145, 2012.

[9] B.X. Guan, B. Bhanu, P. Talbot, & S. Lin, "Detection of non-dynamic blebbing single unattached human embryonic stem cells," in *IEEE International Conference on Image Processing*, pp. 2293-2296, Sept. 2012.

[10] B.X. Guan, B. Bhanu, P. Talbot, & S. Lin, "Automated human embryonic stem cell detection," in *Proc. 2nd IEEE International Conf. On Health Informatics, Imaging and System Biology*, pp. 75-82, Sept. 2012.

[11] Z. Yin, R.Bise, T. Kanade and M. Chen, "Cell segmentation in microscopy imagery symposium on biomedical imaging," in *ISBI*, pp. 125-128, 2010.

[12] R. Adams and L. Bischoff, "Seeded region growing," in *IEEE Trans. PAMI*, vol. 16, no. 6, pp. 641-647, June 1994.

[13] Y. Sun and B. Bhanu, "Reflection symmetry-integrated image segmentation," in *IEEE Trans. Pattern Analysis and Machine Intelligence*, vol. 34, no. 9 , pp. 1827-1841, Sept. 2012.

[14] J. Shi and J. Malik, "Normalized cuts and image segmentation," in *IEEE Trans. PAMI*, vol. 22, no. 8, pp. 888-905, Aug. 2000.

[15] D. Comaniciu and P. Meer, "Mean Shift: A robust approach toward feature space analysis," in *IEEE Trans. Pattern Analysis and Machine Intelligence*, vol. 24, no. 5, pp. 603-619, May 2002.

[16] P. Meer and B. Georgescu, "Edge detection with embedded confidence," in *IEEE Trans. Pattern Anal. Machine Intelligence*, vol. 23, no. 12, pp. 1351-1365, December 2001.

[17] C. Christoudias, B. Georgescu and P. Meer, "Synergism in low level vision," in *IEEE 16th International Conference on Pattern Recognition*, vol. 4, pp. 150-155, 2002.

[18] F. Meyer, "Topographic distance and watershed lines," in *Signal Processing*, vol. 38, pp. 113-125, July 1994.

[19] P. Soille, Morphological Image Analysis: Principles and Applications, Springer-Verlag, pp. 170-171, 1999.

[20] E. W. Weisstein, "Least Squares Fitting," From MathWorld--A Wolfram Web Resource, [Online]. Available: http://mathworld.wolfram.com/LeastSquaresFitting.html. [Accessed 10 Jan. 2015].

[21] E. W. Weisstein, "Statistical Distributions," From MathWorld--A Wolfram Web Resource, [Online]. Available: http://mathworld.wolfram.com/topics/StatisticalDistributions.html. [Accessed 10 Jan. 2015].

[22] R.C. Gonzalez and R.E. Woods, Digital Image Processing: Third Edition, Upper Saddle River, NJ: Pearson Education Inc., pp. 689-794, 2008.

[23] "Biostation-IM," Nikon, [Online]. Available: http://www.nikoninstruments.com/Products/Light-Microscope-Systems/Live-Cell-Screening-Systems/BioStation-IM. [Accessed 10 Jan. 2015].

[24] P. Talbot, N. zur Nieden, S. Lin, I. Martinez, B.X. Guan and B. Bhanu, "Use of video bioinformatic tools in stem cell toxicology," in *Handbook on Nanotoxicology, Nanomedicine and Stem Cell Use in Toxicology*, April 2013.

[25] M. Pepe, G.M. Longton, and H. Janes, "Comparison of receiver operating characteristics curves," UW Biostatistics Working Paper Series- Working Paper 323[eLetter] January 2008. [Online]. Available:

http://biostats.bepress.com/uwbiostat/paper323. [Accessed 10 Jan. 2015].

[26] D. W. Shattuck, S. R. Sandor-Leahy, K. A. Schaper, D. A. Rottenberg and R. M. Leahy, "Magnetic resonance image tissue classification using a partial volume model," in *NeuroImage*, Vol. 13, pp. 856-876, 2001.

[27] T. F. Cootes, C. J. Taylor, D. H. Cooper and J. Graham, "Active shape models – their training and application," *Computer Vision and Image Understanding*, Vol. 61, No. 1, pp. 38-59, January 1995.

[28] S. Zhang, Y. Zhan, M. Dewan, J. Huang, D. N. Metaxas, X. S. Zhou, "Towards robust and effective shape modeling: Sparse shape composition," *Medical Image Analysis*, Vol. 16, No. 1, pp. 265-277, 2012.

Benjamin X. Guan received the B.S. degree with high honor in June 2008 and M.S. degree in December 2009 in Electrical Engineering from the University of California, Riverside. He is currently pursuing his Ph.D. degree in Electrical Engineering at the University of California, Riverside. His research interests are human embryonic stem cell segmentation, detection and classification. He received the Best Paper Award from the IEEE International Conference on Health Informatics, Imaging and System Biology in 2012. He is a member of the IEEE.

Bir Bhanu (S'72 -- M'82 -- SM'87 -- F'95) received the S.M. and E.E. degrees in electrical engineering and computer science from the Massachusetts Institute of Technology, Cambridge, MA, USA; the Ph.D. degree in electrical engineering from the University of Southern California, Los Angeles, CA, USA; and the M.B.A. degree from the University of California, Irvine, CA. Dr. Bhanu is a Distinguished Professor of electrical and computer engineering, and serves as the Founding Director of the Interdisciplinary Center for Research in Intelligent Systems, University of California at Riverside (UCR), Riverside, CA. In addition, he serves as the Director of the National Science Foundation (NSF) Interdisciplinary Graduate Education, Research, and Training Program in video bioinformatics, Interim Chair Department of Bioengineering (since July 2014) and the Director (since 1991) of Visualization and Intelligent Systems Laboratory. He was the founding faculty in the Bourns College of Engineering and the founding Professor of electrical engineering with UCR, and served as its First Chair from 1991 to 1994. Since 1991, 2006, and 2008, he has been a Cooperative Professor of computer science and engineering, bioengineering, and mechanical engineering, respectively, with UCR. He was a Senior Honeywell Fellow with Honeywell Inc., Minneapolis, MN, USA. He has been with the Faculty of the Computer Science, University of Utah, Salt Lake City, UT, USA, and with Ford Aerospace and Communications Corporation, Newport Beach, CA; French Institute for Research in Computer Science and Control (INRIA); and IBM San Jose Research Laboratory, San Jose, CA. He has been the Principal Investigator of various programs for the NSF, the Defense Advanced Research Projects Agency (DARPA), NASA, the Air Force Office of Scientific Research, the Office of Naval Research, the Army Research Office, and other agencies and industries in the areas of video networks, video understanding, video bioinformatics, learning and vision, image understanding, pattern recognition, target recognition, biometrics, autonomous navigation, image databases, and machine-vision applications. He is the coauthor of the books Computational Learning for Adaptive Computer Vision (to be published), Human Recognition at a Distance in Video (Berlin, Germany: Springer-Verlag, 2011), Human Ear Recognition by Computer (Berlin, Germany: Springer-Verlag, 2008), Evolutionary Synthesis of Pattern Recognition Systems (Berlin, Germany: Springer-Verlag, 2005), Computational Algorithms for Fingerprint Recognition (Norwell, MA: Kluwer, 2004), Genetic Learning for Adaptive Image Segmentation (Norwell, MA: Kluwer, 1994), and Qualitative Motion Understanding (Norwell, MA: Kluwer, 1992). He is the coeditor of Video Bioinformatics - From Live Imaging to Knowledge (Springer Computational Biology Series, 2015), Computer Vision Beyond the Visible Spectrum (Berlin, Germany: Springer-Verlag, 2004), Distributed Video Sensor Networks (Berlin, Germany: Springer-Verlag, 2011), and Multibiometrics for Human Identification (Cambridge, U.K.: Cambridge University Press, 2011). He is the holder of 18 (five pending) U.S. and international patents. He has more than 475 reviewed technical publications, including over 135 journal papers and 44 book chapters. Dr. Bhanu is a Fellow of the Institute of Electrical and Electronics Engineers (IEEE), American Association for the Advancement of Science, the International Association of Pattern Recognition, Fellow of American Institute of Medical and Biological Engineering (AIMBE) and the International Society for Optical Engineering. He has served as the General Chair for the IEEE Conference on Computer Vision and Pattern Recognition (CVPR), the IEEE Conference on Advanced Video and Signal-Based Surveillance, the Association for Computing Machinery/IEEE Conference on Distributed Smart Cameras, the DARPA Image Understanding Workshop, the IEEE Workshops on Applications of Computer Vision (founded in 1992, now Winter Applications of Computer Vision Conference), and the CVPR Workshops on Learning in Computer Vision and Pattern Recognition, Computer Vision Beyond the Visible Spectrum, and Multi-Modal Biometrics. He has been on the Editorial Board of various journals and has edited special issues of several IEEE Transactions, such as the IEEE TRANSACTIONS ON PATTERN ANALYSIS AND MACHINE INTELLIGENCE, IEEE TRANSACTIONS ON IMAGE PROCESSING, IEEE TRANSACTIONS ON SYSTEMS, MAN, AND CYBERNETICS -- PART B: CYBERNETICS, IEEE TRANSACTIONS ON ROBOTICS AND AUTOMATION, AND IEEE TRANSACTIONS ON INFORMATION FORENSICS AND SECURITY. He served on the IEEE Fellow Committee from 2010 -- 2012. He was the recipient of the Best Conference Papers and Outstanding Journal Paper Awards, and the Industrial and University Awards for Research Excellence, Outstanding Contributions, Team Efforts and Doctoral/Dissertation Advisor/Mentor Award.

Prue Talbot is a Professor of Cell Biology and the Director of the UCR Stem Cell Center and Core. Her lab is interested in using stem cells to prevent disease and in the effects of tobacco products on human health, including prenatal development. Some of her recent projects have included working with engineers to develop video bioinformatics tools to study morphological and dynamic changes in stem cells during growth and differentiation under normal and stressful conditions and to be able to predict adverse reactions of cells to chemical treatments.

Nikki Jo-Hao Weng received the B.S. degree in Chang Gung University, Taiwan. She is currently a Ph.D student in the cell, molecular and developmental biology program at UC Riverside. She also participates in the UC Riverside NSF integrated graduated education research and training program (IGERT) on video bioinformatics.